

We are IntechOpen, the world's leading publisher of Open Access books Built by scientists, for scientists

6,900

Open access books available

186,000

International authors and editors

200M

Downloads

Our authors are among the

154

Countries delivered to

TOP 1%

most cited scientists

12.2%

Contributors from top 500 universities



WEB OF SCIENCE™

Selection of our books indexed in the Book Citation Index
in Web of Science™ Core Collection (BKCI)

Interested in publishing with us?
Contact book.department@intechopen.com

Numbers displayed above are based on latest data collected.
For more information visit www.intechopen.com



Mechanical Behaviour of Commercial Aluminium Wrought Alloys at Low Temperatures

R. Schneider, B. Heine and R.J. Grant

Additional information is available at the end of the chapter

<http://dx.doi.org/10.5772/58362>

1. Introduction

For a long time, aluminium wrought alloys have been used as the predominant material for the sheet metal processing industry. Aluminium alloys not only show a high affinity for passivation which results in corrosion resistance in many environments [1], but also indicate high specific strengths (strength versus density) and rigidity (Young's modulus versus density). The most commonly used aluminium alloys in aircraft applications of the non-precipitation hardenable groups are EN AW-3xxx, EN AW-5xxx and of the precipitation hardenable groups EN AW-2xxx, EN AW-6xxx and EN AW-7xxx. The advantages of the EN AW-2xxx group are good mechanical properties which remain at higher temperatures, whereas the EN AW-7xxx groups show good mechanical properties at lower temperatures and high stress corrosion resistivity. A negative aspect is, however, that aluminium alloys have a very low formability when compared with modern steels. Figure 1 illustrates the fracture elongation versus yield strength of aluminium wrought alloys and deep drawing steels in optimised hardened condition. Aluminium wrought alloys with the designation EN AW-7xxx series in peak-aged condition show yield strength values comparable with the micro-alloyed steels; although the fracture elongation differs slightly in favour of the steels.

Yield strength values from the wrought alloys of EN AW-6xxx group reach only about 50% of the strength which can be obtained from the EN AW-7xxx group at ambient temperatures; both aluminium wrought alloys are precipitation hardenable in peak-aged condition. The fracture elongation of the 6xxx and 7xxx group can be identified to be approximately half of the value which can be obtained using bake-hardening steels. Yield strength values from non-heat-treatable, and therefore only strain-hardenable, aluminium alloys of the EN AW-5xxx group are slightly higher when present in highly strain-hardened condition (e.g. H18). But their fracture elongation values in an annealed condition are equivalent to those exhibited by

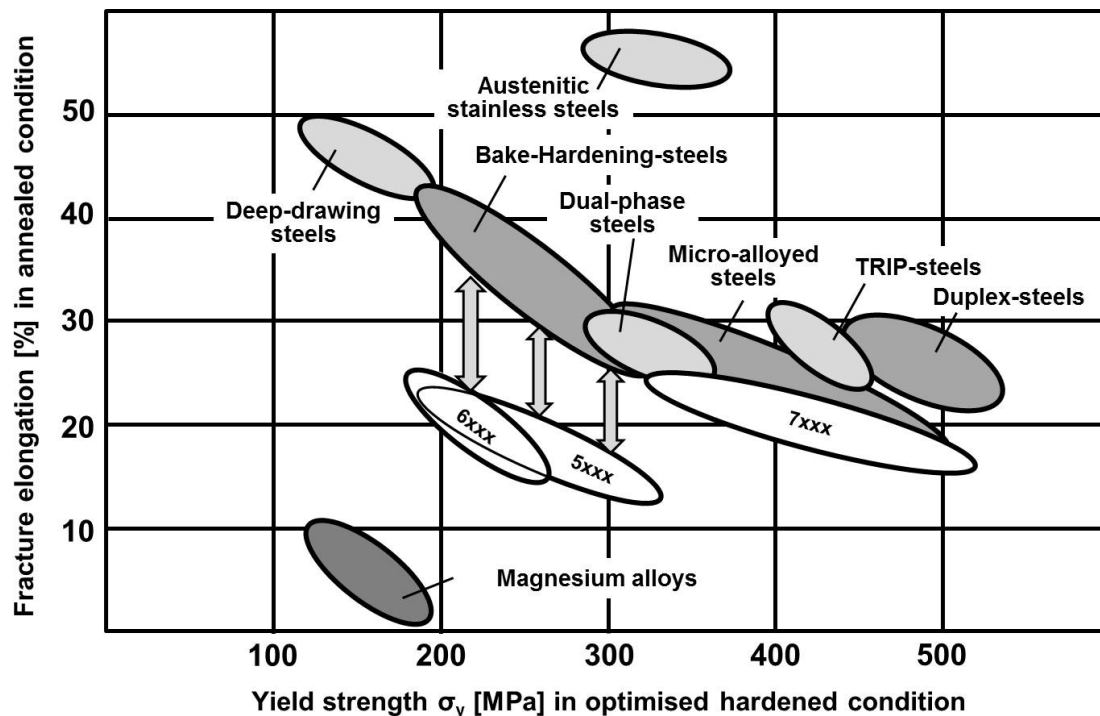


Figure 1. Fracture elongation for aluminium wrought alloys of the EN AW-5xxx, EN AW-6xxx and EN AW-7xxx series at $T=298$ K and deep-drawing steels at $T=298$ K. Yield strength in an optimised hardened condition for all mentioned groups at $T=298$ K.

the EN AW-6xxx group. So, ways of enhancing the fracture elongation of wrought aluminium alloys to levels that are at least comparable with those of deep-drawing steels and additionally possess corresponding strength values are sought. Forming aluminium alloys below room temperature would be an approach, where strain hardening losses and precipitation processes are not an issue. In this regard there is no danger of a reduction in strength through the mechanism of recovery, recrystallization and aging which is in most cases induced by forming at higher temperatures. Furthermore, in previous investigations during tensile testing it was observed that in certain aluminium alloys, which were present in various heat treatment conditions, the Lüders and the Portevin-LeChatelier (PLC) effect occurs at room temperature [2] [3]. This PLC effect not only causes a bad surface quality on sheet metals, but also creates a reduction of the uniform elongation and fracture elongation [2]. It is expected that in tensile testing at low temperatures the negative impact caused by the PLC effect can be reduced and therefore the values of uniform elongation and fracture elongation can be increased.

2. Portevin-LeChatelier (PLC) Effect

2.1. Phenomena of the PLC effect

Considering a tensile testing specimen, consisting of an isotropic ductile material, it can be observed that straining in the direction of the principal normal stress is accompanied by a

cross-sectional reduction in width and thickness. In the region of uniform elongation the prismatic geometry of the specimen remains, since a *random localisation* stabilises itself according to the Considère-criteria. Leaving this region of the stress-strain curve and moving into the region which signifies the region of necking behaviour a localised and random reduction in width and thickness results in an overall reduction in cross-section. It is of note that for a tensile specimen, where the width is much greater than the thickness, a reduction in the cross-section only appears at a volume of material inclined at an angle of approximately 55° measured in direction of the principal normal stress. Localised necking predominantly in thickness will finally fracture the specimen when constricted [4] [5]. Testing an annealed aluminium alloy with the designation of EN AW-5xxx shows that a cross-sectional reduction occurs in fact before reaching the necking area. Figure 2 a) shows localised necking over the whole specimen length.

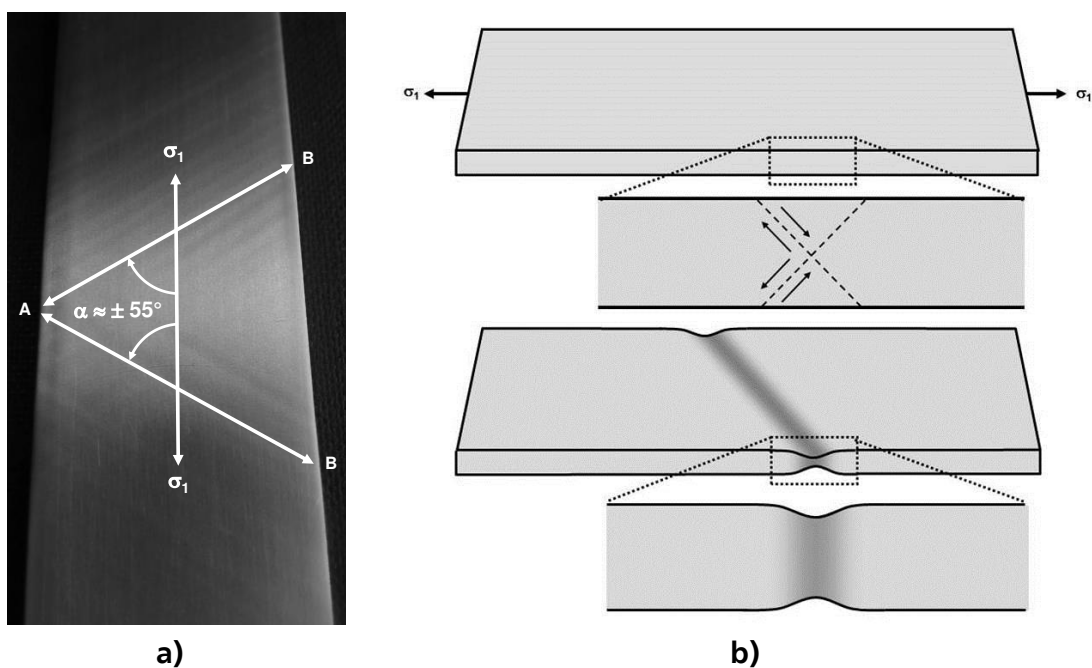


Figure 2. a) Cross-sectional reduction of EN AW-5xxx specimen in annealed condition which shows localised necking at an angle of around 55° measured in direction of principal normal stress before reaching the necking area. b) Schematic cross-sectional reduction in thickness co-occurring with shear deformations in several planes.

In this deformation state it can be observed that only localised necking occurs (\overline{AB}) and there is no reduction in width over the whole specimen length (\overline{BB}) which would be denoted as diffuse necking [6]. This is **in contrast** to most metallic materials, where localised through-thickness necking arises e.g. on aluminium alloy EN AW-5xxx in an annealed condition, but not over the whole length. As a consequence, a pattern of localised through-thickness striations can be observed oriented at around $\pm 55^\circ$ to the direction of the principal normal stress (Figure 2 a)) [2] [3]: these are also known as PLC bands. Figure 2 b) illustrates a formation of this localised affect which is co-occurring with shear deformations in several planes. The condition

of the volume of material where localised necking arises is that no strain be imposed on the non-deforming material adjacent to the flowing section which leads to $d\varepsilon_w' = 0$ as illustrated in Figure 3 [6]. The localising volume only deforms in thickness ($d\varepsilon_t$) and lengthways ($d\varepsilon_l'$), which characterises a biaxial strain state. Provided that there is an ideal plastic material behaviour and a negligible elastic fraction compared with the plastic fraction, Lévy-von Mises equations can be applied.

$$\frac{d\varepsilon_l}{\sigma_1 - \frac{1}{2} \cdot (\sigma_2 + \sigma_3)} = \frac{d\varepsilon_w}{\sigma_2 - \frac{1}{2} \cdot (\sigma_3 + \sigma_1)} = \frac{d\varepsilon_t}{\sigma_3 - \frac{1}{2} \cdot (\sigma_1 + \sigma_2)} \quad (1)$$

let $\sigma_1 \neq 0$ and $\sigma_2 = \sigma_3 = 0$ then

$$\frac{d\varepsilon_l}{\sigma_1} = \frac{d\varepsilon_w}{-\frac{1}{2} \cdot \sigma_1} = \frac{d\varepsilon_t}{-\frac{1}{2} \cdot \sigma_1} \quad (2)$$

If only $d\varepsilon_l$ and $d\varepsilon_w$ are considered (because of a small sheet thickness), the expression can be rewritten as

$$d\varepsilon_l = -2 \cdot d\varepsilon_w \quad (3)$$

Since $d\varepsilon_w < 0$ a Mohr's circle of strain can be developed as illustrated in Figure 3. Applying a coordinate transformation it can be shown that $\alpha = 70^\circ 32'$ if $d\varepsilon_w' = 0$.

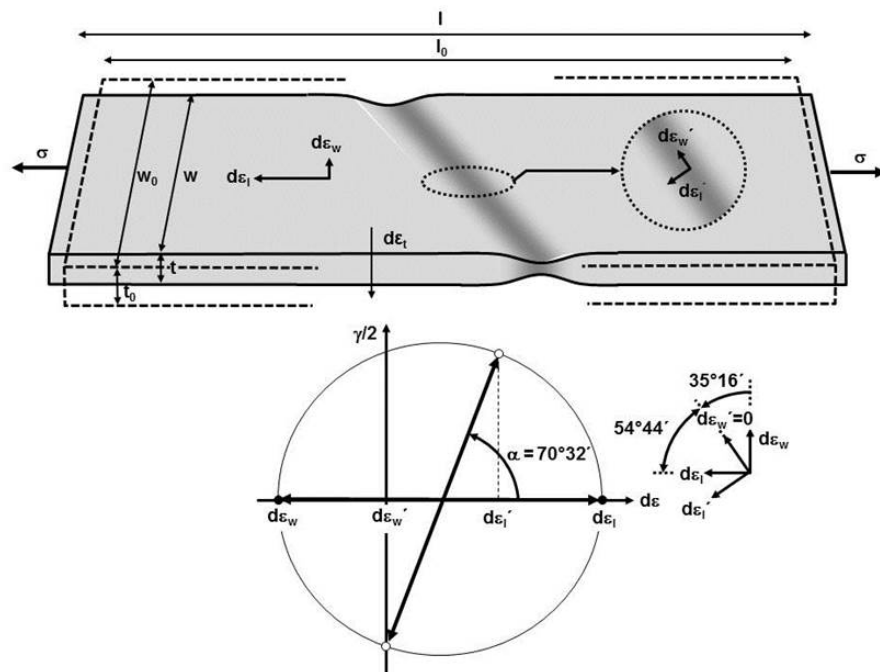


Figure 3. Cross-sectional reduction of a flat specimen according Mohr's circle of strain

Thus, the angle between the direction of the localised neck and the direction of the principal normal stress is ideally $54^{\circ}44'$ which is in accordance with the hypothesis of Hill [7]. Eventual variations can be attributed to textures of the material.

2.2. Microscopic background of the PLC-effect

The microscopic background of the PLC effect is still a subject of discussion. This is because the PLC effect appears at temperatures where interstitial or substitutional diffusion of solute alloying elements do not offer sufficient mobility by bulk diffusion. A brief introduction of the development of ideas concerning the PLC effect is illustrated in [8] [9]. The first model developed by Cottrell and Bilby [10] assumed that the mobility of solute atoms is actually high enough to follow mobile dislocations. Subsequently, McCormick recognised that the mobility of solute atoms is barely sufficient to follow mobile dislocations, and he postulated that clustering mobile dislocations only occurs if they are arrested by obstacles such as by forest dislocations, for example [11]. Van den Beukel presupposed in his model, which was based on McCormick's work, that arresting mobile dislocations at forest dislocations is only caused by volume diffusion of solute atoms [12]. Following a proposal of Sleeswyk [13], the model created by Mulford [14] not only postulates the arresting of the stopped dislocation by volume diffusion, but additionally by a simultaneously running pipe diffusion (see Figure 4).

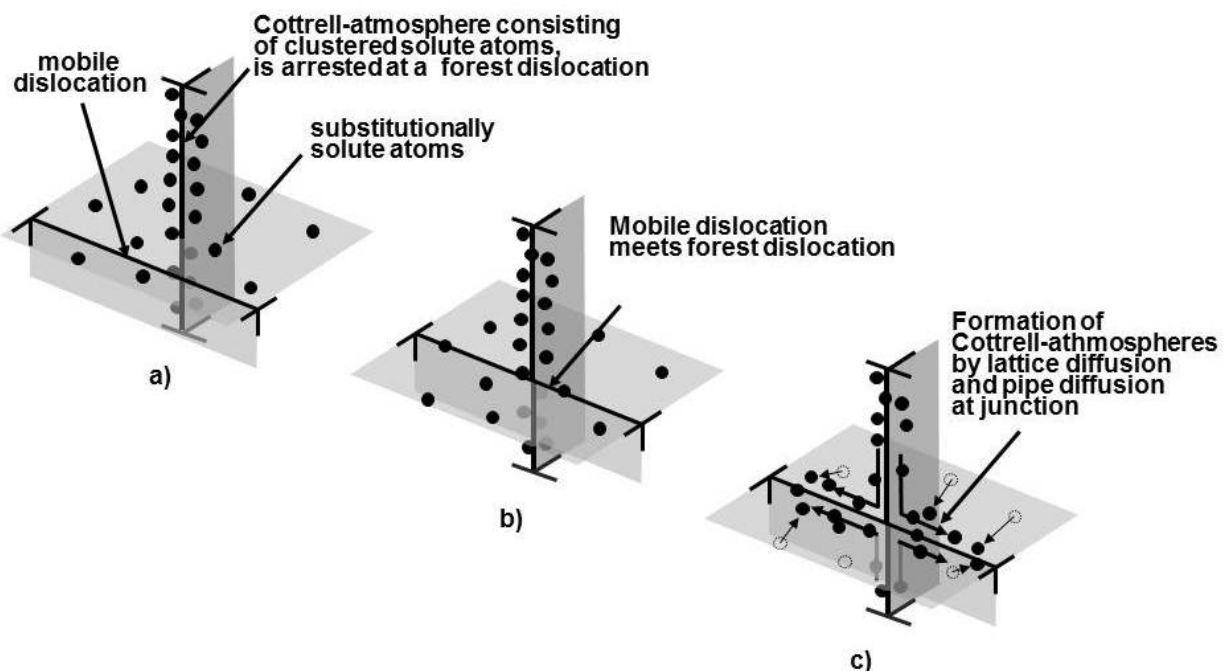


Figure 4. Substitutional solute atoms at stationary forest dislocations generate Cottrell-atmospheres, whose atoms cluster at a mobile dislocation which meets a forest dislocation via pipe diffusion.

A requirement for such a condition is a prior formation of a Cottrell-atmosphere at stationary forest dislocations. The pipe diffusion occurs without the acceleration caused by the vacancy mechanism. Modelling the pipe diffusion of the substitutionally dissolved magnesium in the

aluminium bulk showed that the effectiveness of this diffusion process is not high enough to explain the experimental results [9]. As a consequence of this model the diffusion velocity of magnesium atoms is too slow to form Cottrell-atmospheres around the core of the arrested dislocation during representative times. Considering these results Picu [8] developed a new model which is based on the estimation that a forest dislocation embedded in a Cottrell-atmosphere reacts with a mobile dislocation by forming *dislocation jogs*. The higher the intensity of Cottrell-atmosphere around a forest dislocation the greater the energy necessary for forming jogs.

3. Experimental methods

A set of experimental tests were conducted based around a tensile test machine. Four types of wrought aluminium alloys were examined which are detailed in Table 1. In this table the sheet thickness and detailed composition are shown.

	EN AW-1050A	EN AW-5182	EN AW-6016	EN AW-7021
Condition	H14	H111	W ₃₀ - T4	T4
Temper [15]	H14 strain-hardened to a half hard condition - no thermal treatment	H111 slightly strain- hardened (less than H11) – no thermal treatment	solution heat-treated at 465°C for 20 minutes and naturally aged to a substantially stable condition	W30 solution heat-treated at 465°C for 20 minutes and tested within 30 minutes
Specimen thickness [mm]	0,95	1,15	1,15	0,95
Si [wt.-%]	0,25	0,20	1,20	0,07
Fe [wt.-%]	0,40	0,35	0,40	0,16
Cu [wt.-%]	0,05	0,15	0,15	0,12
Mn [wt.-%]	0,05	0,35	0,15	0,02
Mg [wt.-%]	0,05	4,40	0,40	-
Cr [wt.-%]	-	0,10	0,10	-
Zn [wt.-%]	0,07	0,25	0,15	6,24
Ti [wt.-%]	0,05	0,10	0,15	0,02
Zr [wt.-%]	-	-	-	0,14

Table 1. Heat treatment, thickness and chemical composition of tested aluminium alloys

For the purpose of evaluating potential strain rate dependencies the uniaxial tensile tests for the aluminium alloys EN AW-6016 and EN AW-7021 in the solid solution heat treated and naturally aged condition T4, and the EN AW-5182 aluminium alloy in the strain hardened condition H111 (as currently implemented in industrial applications), were carried out with the following three forming velocities; $v_1=200\text{mm}/\text{min}$ (maximum velocity of the tensile testing machine), $v_2(\frac{1}{4}v_1)=50\text{mm}/\text{min}$ and $v_3(\frac{1}{10}v_2)=5\text{mm}/\text{min}$ resulting in strain rates $\dot{\epsilon}_1(v_1)=6.60 \times 10^{-2} \text{ s}^{-1}$, $\dot{\epsilon}_2(v_2)=1.70 \times 10^{-2} \text{ s}^{-1}$ and $\dot{\epsilon}_3(v_3)=0.17 \times 10^{-2} \text{ s}^{-1}$ respectively (see Table 2). By way of comparison, the highest strain rate illustrated, v_1 , approaches the forming velocity used in a typical industrial process. Determining the effect of precipitations for the 6000 and 7000 series a number of subsequent tests with the highest strain rate $\dot{\epsilon}_1$ were carried out within 30 minutes after a solid solution heat treatment (W_{30} condition). As a reference the aluminium alloy EN AW-1050A was tested in half-hard condition (H14) with $\dot{\epsilon}_1$. To be thorough regarding a potential influence of the strain rates, the reference aluminium alloy was also tested with the lowest strain rate ($\dot{\epsilon}_3$)

Aluminium alloy	condition	strain rates		
		$6.60 \cdot 10^{-2} \text{ s}^{-1}$	$1.70 \cdot 10^{-2} \text{ s}^{-1}$	$0.17 \cdot 10^{-2} \text{ s}^{-1}$
EN AW-1050A	H14	X		X
EN AW-5182	H111	X	X	X
EN AW-6016	W_{30}	X		
	T4	X	X	X
EN AW-7021	W_{30}	X		
	T4	X	X	X

Table 2. Different strain rates used in the experiment

Flat sheet specimens were CNC machined showing a test section width of 12.5mm in accordance with DIN EN ISO 6892-1 (A_{50}) [16]. Attention was given towards the rolling direction of the sheet metal which was perpendicular to the applied load. The length of the 50mm wide clamp sections of the specimens were designed to fit with the requirements of the cryogenic set-up.

A specially designed cryogenic dewar (Figure 5) was used to obtain and maintain the sub-zero temperatures required in these tests. A variation of testing temperatures was reached by way of a *medium-pipe*, which was used as a vessel carrying isothermal media, and was cooled by liquid nitrogen. The isothermal media used for the experiment shown in Table 3 were first pre-cooled in an external chamber. The final temperature was reached in the cryogenic dewar, where the specimen remained for around 5 minutes, before the test started. Furthermore,

homogeneity of the temperature within the medium-pipe was accomplished by injecting inert gas. In case of a sudden temperature drop the chamber included an inlet for compressed air, which ensured a replacement of the cold environment between medium-pipe and cryogenic dewar. The investigations were conducted using a type Z100 tensile testing machine from Zwick.

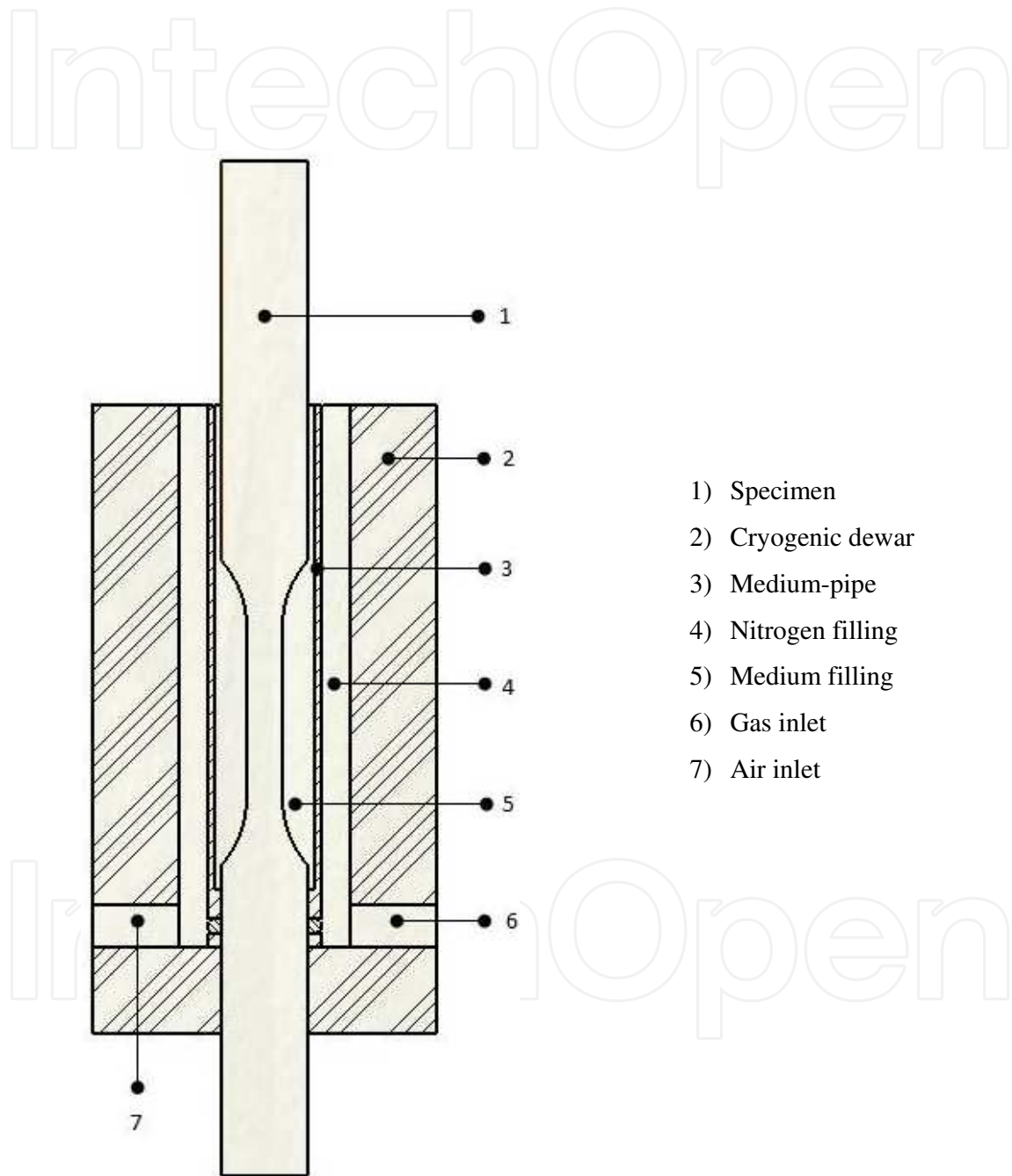


Figure 5. Cryogenic set-up

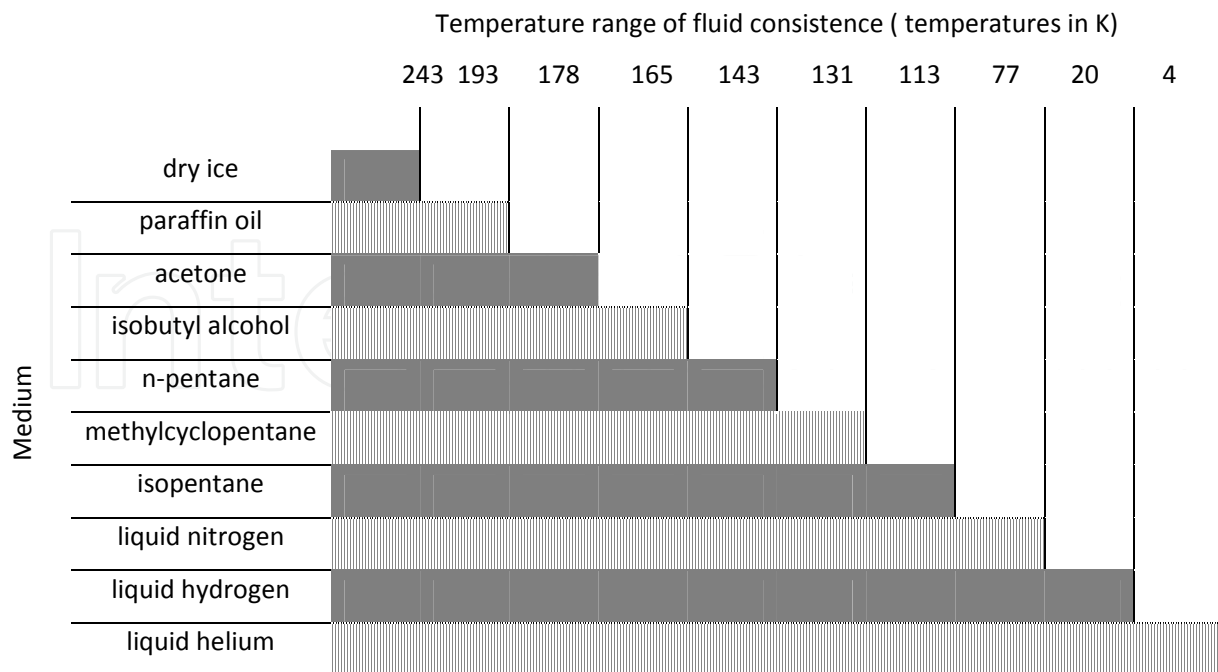


Table 3. Application temperature for different media [17]

4. Results

Figure 6 a) through f) shows for the aluminium alloys tested the temperature dependency of the yield strength σ_y , ultimate tensile strength (UTS), uniform elongation e_u and fracture elongation e_f which was determined at a strain rate of $6.60 \times 10^{-2} \text{ s}^{-1}$.

It can be seen that with one exception and for all materials the yield strength, ultimate tensile strength and elongation rises consistently when temperature is decreased. The strength values of the aluminium alloys in W_{30} condition are lower than in T4 condition, which is as expected. For the aluminium alloys EN AW-5182 and EN AW-7021 in W_{30} condition a uniform elongation of over 40% and a fracture elongation of considerably more than 50% can be reached at 77K. A similar trend can be observed for the aluminium alloy EN AW-6016 in both heat treatment conditions, where the elongation in T4 condition is less than in W_{30} condition. For a decrease in temperature the aluminium alloy EN AW-1050A shows a rather shallow rise of the ultimate and yield strengths over the whole temperature range; whereas curves of uniform and fracture percentage elongation of this alloy indicate significant increases in the magnitudes of their gradients. The strength and elongation of the aluminium alloys EN AW-7021 also show a growing trend if temperature is reduced. For both heat treatment conditions, T4 and W_{30} , a gradual elongation rise of 25% at 152 K can be seen. If the temperature is lower than 152 K the elongation of the peak aged aluminium (T4) alloy decreases again. In turn, when present in W_{30} condition, the uniform elongation rises to more than 40% and the fracture elongation approaches 50% at 77K.

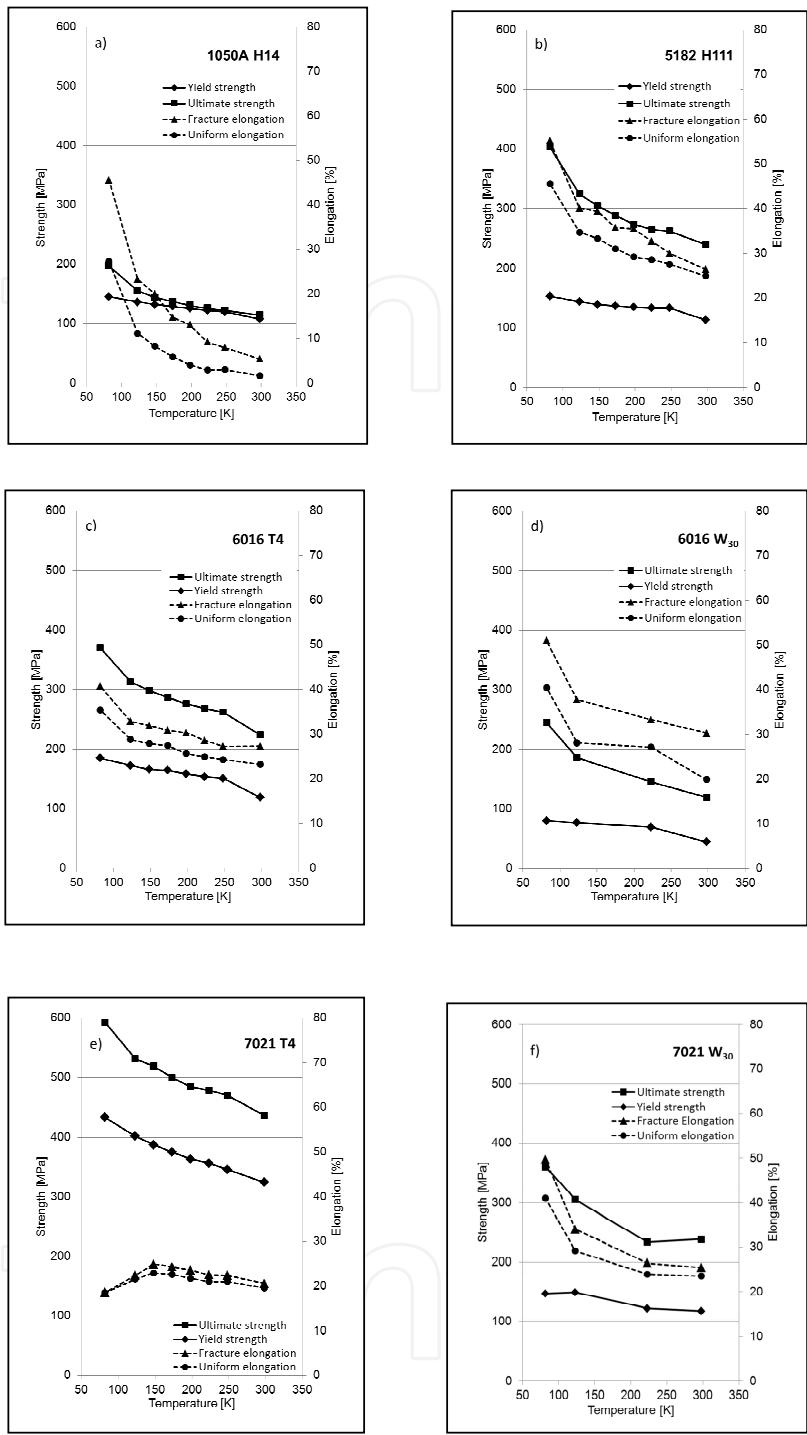


Figure 6. Temperature dependence of the yield strength σ_y , ultimate tensile strength UTS, uniform elongation e_u and fracture elongation e_f , which was determined at a strain rate of $6.60 \cdot 10^{-2} \text{ s}^{-1}$.

The influence of strain rates regarding strength values can be considered as small (see Figure 7 a), c), e) & g)). A slightly more distinct effect can be observed for the elongation values, especially for EN AW-5182 and EN AW-6016 T4. Nevertheless, those variations converge as the temperature approaches 77K (see Figure 7 b), d), f)&g)).

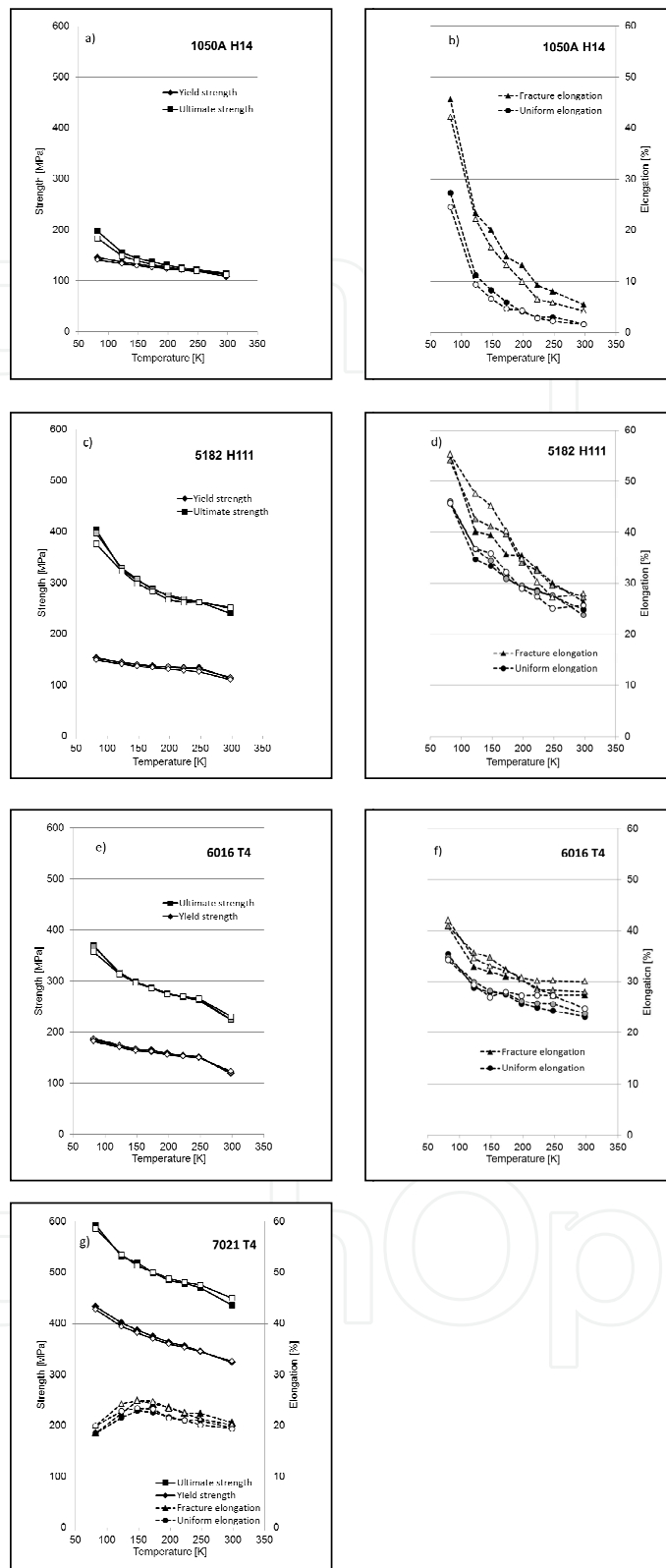


Figure 7. Temperature dependency of yield strength, ultimate strength and fracture elongation at different strain rates (black icon $6.60 \times 10^{-2} \text{ s}^{-1}$, grey icon $1.70 \times 10^{-2} \text{ s}^{-1}$, white icon $0.17 \times 10^{-2} \text{ s}^{-1}$)

Some overall observations were made as a result of the tests from stress-strain data. Firstly aluminium alloy EN AW-1050A-H14 showed no pronounced yielding for all strain rates and temperatures. The same effect was observed for EN AW-6016 in both heat treatment conditions, T4 and W_{30} . In contrast the aluminium alloy EN AW-5182-H111 showed pronounced yielding at all strain rates and temperatures. Aluminium alloy EN AW-7021 in W_{30} condition indicated pronounced yielding only at 298K and 248K. When the temperature was reduced this effect was not evident. On the other hand, EN AW-7021 in T4 condition showed similar yielding effects for all strain rates as was also observed for EN AW-6016. If one now considers Figure 8, the results of increasing the uniaxial load on an EN AW-5182-H111 specimen can be seen over the elastic and plastic regions. It is clear that there is a pronounced yielding behaviour accompanied by a region of stress oscillations. For the results, shown at $T=298\text{K}$, the amplitude is as high as $\pm 2\text{ MPa}$; whereas for $T \leq 248\text{K}$ the magnitude reduces to $\pm 0.2\text{ MPa}$.

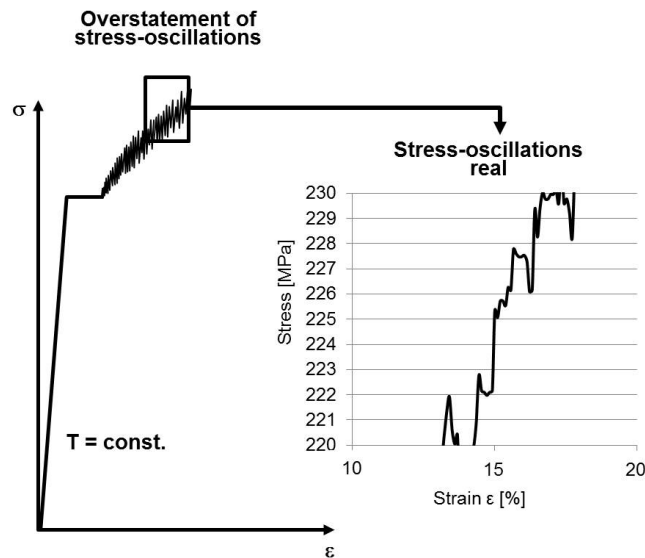


Figure 8. Pronounced yielding and stress amplitudes in the plastic region of EN AW-5182

5. Discussion

The PLC-effect, caused by Cottrell-atmospheres, offers a plausible mechanism to explain the resulting reduction of fracture elongation e_f and uniform elongation e_w , which leads to a decrease in the strain hardening coefficient n . The intensity of Cottrell-atmospheres is proportional to the quantity of dissolved atoms with a sufficiently high diffusivity, and the time to form Cottrell-atmospheres. Thus, in the case of the precipitation hardenable alloy EN AW-6016 and EN AW-7021, it was intended to increase the amount of dissolved atoms via solution heat-treatment, quenching and immediate testing of the mechanical properties at this condition. Comparing the two heat-treatment conditions T4 and W_{30} , it can be seen in Figure 6 c) through f) that this procedure had the expected positive effect on fracture elongation e_f

and uniform elongation e_u . It seems that the dissolved atoms had not the opportunity to form Cottrell-atmospheres which confirms the assertion of [8]. If the temperature is reduced, the diffusivity of the dissolved atoms is generally decelerated. Therefore, the formation of Cottrell-atmospheres, of the same intensity during the same period of time, is unlikely: this would correspond to a reduced PLC-effect. Figure 7 b), d) & f) illustrates this effect in terms of a growth in the fracture elongation e_f and uniform elongation e_u ; thereby, the strain hardening coefficient n rises simultaneously as illustrated in Figure 9 a), b), c), d) & f). The overall increase in strength throughout the tested aluminium alloys could be explained *inter alia* by the activation energy which reduces as temperature is lowered. Consequently, the force needed to move a dislocation through the crystal lattice (Peierls Nabarro force), reaches a maximum as temperature converges to 0 K [4] [18].

Ludwik, Hollomon and Backofen identified that the flow stress K_f can be elevated by raising the strain ε as well as lifting the strain rate $\dot{\varepsilon}$ [19]. The general relationship between the physical values is:

$$K_f = K_f(\varepsilon, \dot{\varepsilon}) \quad (4)$$

A relationship which was empirically developed by Ludwik modified by Hollomon and extended by Backofen is

$$K_f = c \cdot \varepsilon^n \cdot \dot{\varepsilon}^m \quad (5)$$

where c is a material dependent constant (strength coefficient), n being the strain-hardening coefficient and m represents the strain rate sensitivity parameter. At temperatures where a metallurgical softening takes place to a limited extent ($T \leq 0.4T_m$; T_m =melting point [K]), an increase of the strain rate will not affect the true stress. Therefore, the m value can be assumed to be much smaller than 1. The results in Figure 7 confirm this statement.

If m is set to be 0 it follows:

$$K_f = c \cdot \varepsilon^n \quad (6)$$

Using this relationship most stress-strain curves can be described accurately in the region of uniform elongation at $T \leq 0.4T_m$. As exemplified in Heiser [5] the strain hardening coefficient n can be written as true uniform strain ε_u or related to the uniform elongation e_u .

$$n = \varepsilon_u = \ln(1 + e_u) \quad (7)$$

The strain hardening coefficient n describes to what extent a material can be deformed before localised necking will start, i.e. the flow curve. Figure 9 shows correlations between experimental evaluated strain hardening coefficients using Eq. (7) and uniform elongation e_u in relation to temperature and strain rate of EN AW-1050A, EN AW-5182, EN AW-6016 and EN

AW-7021 specimens. In addition, the Ludwik curve is included which represents n calculated using Eq. (7).

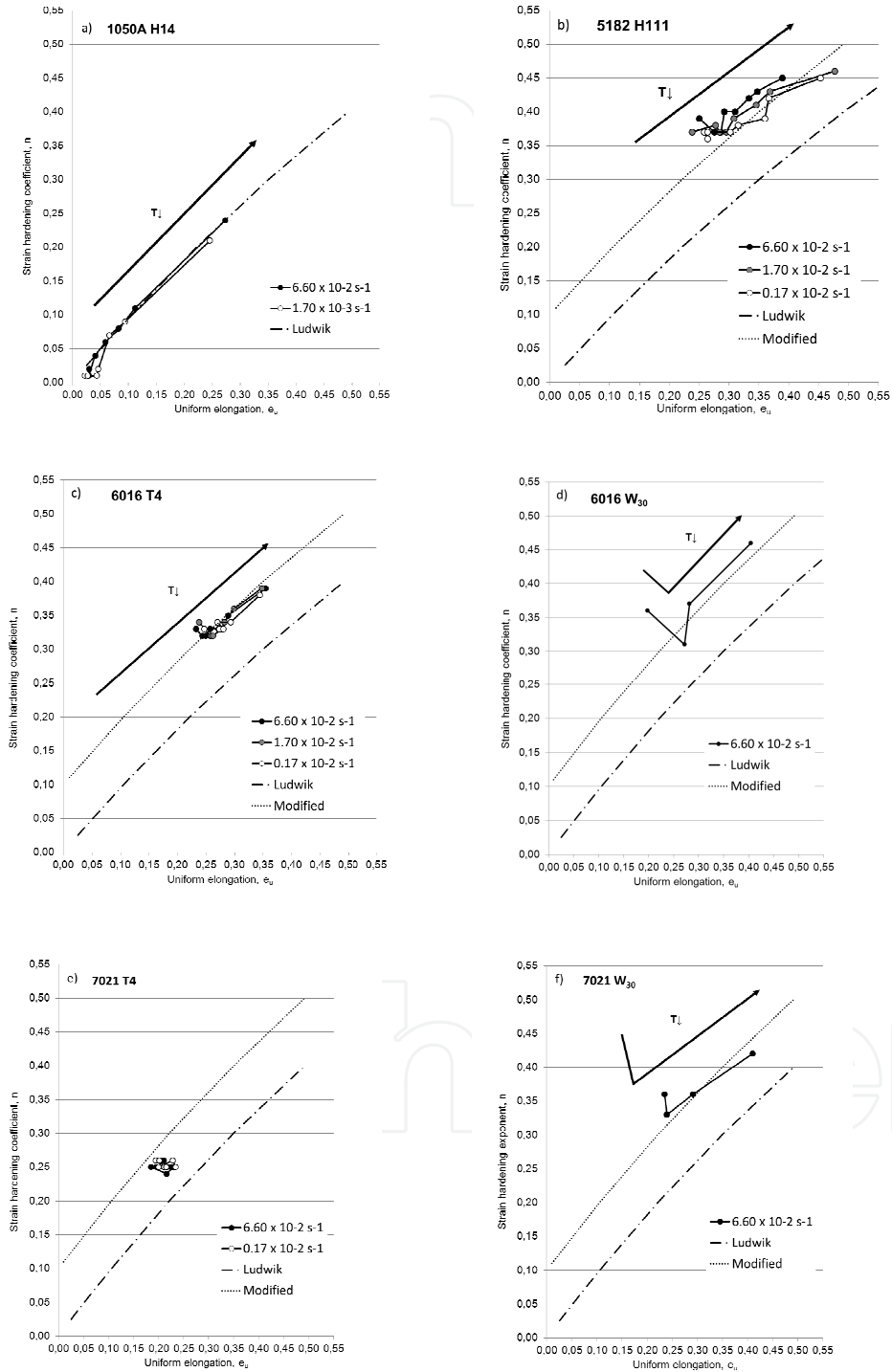


Figure 9. Temperature and strain rate dependence of strain hardening exponent n and uniform strain ϵ_u . Additionally included is the dependence of strain hardening coefficient and uniform elongation after Ludwik if only strain hardening is considered

Figure 9 a) through f) shows only a slight strain rate dependency. Apart from the temperature range between 298K and 248K and from EN AW-7021 in the precipitation hardened condition (T4), an increase of the strain hardening coefficient and uniform elongation as temperature is reduced can be seen. Except for the aluminium alloy 1050A, (Figure 9 a)) which is consistent with the Ludwik curve, tested aluminium alloys indicate a parallel offset. It is assumed that this shift is due to the PLC-effect. Therefore Eq. 6, which takes only the strain hardening process into account, seems not to be applicable for all aluminium alloys. A modification to this equation would seem appropriate to allow for the description of materials which exhibit a PLC-effect. Eq. (8) illustrates a *simple* modification of Eq. (7). The addition of a constant, p , provides a shift to the Ludwik curve and can now be written

$$n = \ln(1 + e_u) + p \quad (8)$$

The modified Ludwik curve is illustrated on Figure 9 b) through f) which incorporates a value of $p=0.1$. Whilst it is clear that the new fit corresponds more appropriately (recalling that the 7021 Figure 9 e) is in a naturally aged condition (T4) and is not in an ideal state for cryogenic forming processes), further analyses of flow curves presented in this and additional studies will provide the basis of a more refined relationship. This will be presented in a subsequent publication.

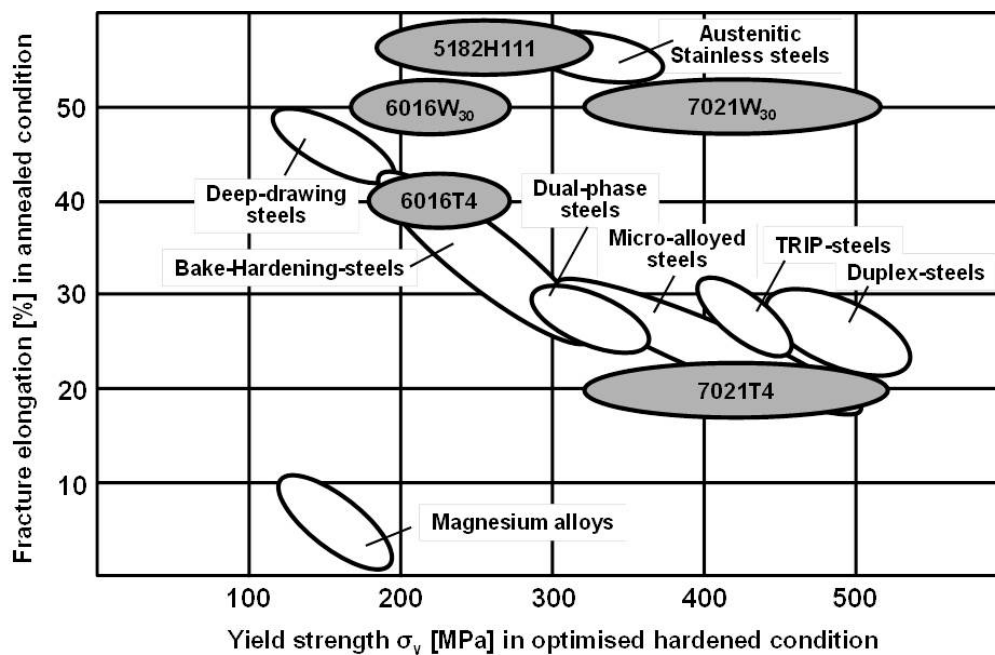


Figure 10. Fracture elongation for aluminium wrought alloys of the EN AW-5xxx, EN AW-6xxx and EN AW-7xxx series at $T=77$ K and deep-drawing steels at $T=298$ K. Yield strength in optimised hardened condition for all mentioned groups at $T=298$ K.

6. Conclusion

The plastic behaviour of commercial aluminium wrought alloys in annealed or solution annealed condition can be positively enhanced if the forming temperature is below 123K. This advantage can be reached without any interference of higher strain rates.

Figure 10 demonstrates the fracture elongation values which are currently attainable from aluminium alloys compared with values achievable from deep-drawing steels. A competitive advantage of cryogenic forming of annealed or solution annealed aluminium alloys is clearly shown. Flow curves showing PLC-effects can be described more precisely with addition of a constant p which represents an extension of the initial Ludwik relationship.

Author details

R. Schneider^{1,2}, B. Heine² and R.J. Grant¹

1 Glyndŵr University, Department of Engineering and Applied Physics, United Kingdom

2 Aalen University of Applied Sciences, Institut für Oberflächen-und Werkstofftechnik, Germany

References

- [1] W. S. Miller, L. Zhuang, J. Bottema, A. J. Wittebrood, P. De Smet, A. Haszler and A. Vieregge, "Recent development in aluminium alloys for the automotive industry," *Mat. Sci. Eng. A280* (2000) 37-49.
- [2] E. Pink and A. Grinberg, "Praktische Aspekte des Portevin-LeChatelier-Effektes (1)," *Aluminium* 60 (1984) 687-691.
- [3] E. Pink and A. Grinberg, "Praktische Aspekte des Portevin-LeChatelier-Effektes (2)," *Aluminium* 60 (1984) 764-768.
- [4] G. E. Dieter, *Mechanical Metallurgy*, London: McGraw-Hill BookCompany (UK) Limited, 1988 pp. 289-291.
- [5] M. Heiser and G. Lange, "Scherbruch in Aluminium-Legierungen infolge lokaler plastischer Instabilität," *Z. Metallkd.* 83 (1992) 115.
- [6] S. P. Keeler and W. A. Backofen, "Plastic instability and fracture in sheets stretched over rigid punches," *Trans. ASM* 56 (1963) 25-48.
- [7] R. Hill, "On discontinuous plastic states, with special reference to localized necking in thin sheets," *J. Mech. Phys. Sol.* 1 (1952) 19-30.

- [8] R. C. Picu, "A mechanism for the negative strain-rate sensitivity of dilute solid solutions," *Acta Mat.* 52 (2004) 3447-3458.
- [9] R. C. Picu, G. Vincze, F. Ozturk, J. J. Gracio, F. Barlat and A. M. Maniatty, "Strain rate sensitivity of the commercial aluminum alloy AA5182-O," *Mat. Sci. Eng. A390* (2005) 334-343.
- [10] A. H. Cottrell and B. A. Bilby, "Dislocation theory of yielding and strain ageing of iron," *Proc. Phys. Soc. A62* (1949) 49-62.
- [11] P. G. Mc Cormick, "A model for the Portevin-Le Chatelier effect in substitutional alloys," *Acta Metall* 20 (1972) 351-354.
- [12] A. van den Beukel, "Theory of the effect of dynamic strain ageing on mechanical properties," *Status Solidi A30* (1975) 197-206.
- [13] A. W. Sleeswyk, "Slow strain hardening of ingot iron," *Acta Metall* 6 (1958) 598-603.
- [14] R. A. Mulford and U. F. Kocks, "New observations on the mechanisms of dynamic strain aging and of jerky flow," *Acta Metall* 27 (1979) 1125-1134.
- [15] DIN EN 515: Aluminium und Aluminiumlegierungen-Halbzeug-Bezeichnung der Werkstoffzustände, Berlin: Beuth Verlag, 1993.
- [16] DIN EN ISO 6892-1: Zugversuch-Metallische Werkstoffe-Prüfverfahren bei Raumtemperatur, Berlin: Beuth Verlag, 2009.
- [17] "IFA Institut für Arbeitsschutz der Deutschen Gesetzlichen Unfallversicherung," GESTIS Substance Database, [Online]. Available: <http://gestis-en.itrust.de> [Accessed 10 02 2014].
- [18] B. Heine, *Werkstoffprüfung Ermittlung von Werkstoffeigenschaften*, München: Carl Hanser Verlag, 2011 pp.170-172.
- [19] J. K. Gregory, *Superplastic deformation in oxide dispersion strengthened nickel base superalloys*, Stanford University: Ph.D. Thesis, 1983.

